TU Delft

Delft University of Technology

# Marchenko Focusing Without Up/Down Decomposition

Wapenaar, C.P.A.

**DOI**
10.1190/segam2020-3423471.1

**Publication date**
2020

**Document Version**
Accepted author manuscript

**Published in**
SEG Technical Program Expanded Abstracts 2020

**Citation (APA)**
Wapenaar, C. P. A. (2020). Marchenko Focusing Without Up/Down Decomposition. In *SEG Technical Program Expanded Abstracts 2020* (pp. 3593-3597). (SEG Technical Program Expanded Abstracts). Society of Exploration Geophysicists. https://doi.org/10.1190/segam2020-3423471.1

**Important note**
To cite this publication, please use the final published version (if applicable).
Please check the document version above.

**Copyright**
Other than for strictly personal use, it is not permitted to download, forward or distribute the text or part of it, without the consent of the author(s) and/or copyright holder(s), unless the work is under an open content license such as Creative Commons.

**Takedown policy**
Please contact us and provide details if you believe this document breaches copyrights.
We will remove access to the work immediately and investigate your claim.

*This work is downloaded from Delft University of Technology.*
*For technical reasons the number of authors shown on this cover page is limited to a maximum of 10.*

# Marchenko Focusing Without Up/Down Decomposition

*Mert S. R. Kiraz & Roel Snieder, Center for Wave Phenomena, Colorado School of Mines*
*Kees Wapenaar, Delft University of Technology*

## SUMMARY

Current Marchenko algorithms require up/down separation, and solving the Marchenko equation enables one to retrieve the up/down components of the Green's function. We propose an iterative scheme to relax the need for up/down separation for focusing. By presenting a visual tour, we show how to retrieve the Green's function in the subsurface at a pre-defined location without requiring component decomposition. Our retrieved Green's function contains accurate primary and multiple events of the heterogeneous subsurface and forms the basis for obtaining an image of the subsurface without the need for up/down decomposition.

## INTRODUCTION

Rose (2001, 2002) describes focusing as finding an incident wave that becomes a delta function at the focus location inside the medium at a given time. Following this work, Broggini and Snieder (2012) utilize Rose's approach for seismic exploration problems and introduce a scheme to retrieve the response to a virtual source inside the medium without requiring an actual source at the virtual source location. The retrieved Green's function contains all internal multiples as well as primary events. This method requires surface-recorded data and an estimate of the direct arrivals, which enables one to specify the virtual source location. One can also retrieve the virtual response by seismic interferometry (Weaver and Lobkis, 2001; Wapenaar et al., 2005).

Retrieving the virtual response at any location in the subsurface is an important technique for creating robust subsurface images and has the potential of eliminating the disturbing effects of the overburden by creating virtual responses whereby complex subsurface structures are eliminated. Marchenko methods (Rose, 2001; Broggini and Snieder, 2012; Broggini et al., 2012, 2014; Wapenaar et al., 2014) exploit the ability to retrieve virtual source information inside the subsurface, resulting in robust subsurface images. The Marchenko method enables one to create virtual sources and receivers in the subsurface at arbitrary depth positions, and only requires surface recorded data and a smooth background velocity model. By introducing initial focusing functions in a reference medium similar to the actual medium, the Marchenko equation can be solved, and the up- and down-going components of the Green's function can be retrieved. The retrieved components can then be used to image the subsurface by applying an imaging condition. The Marchenko method, however, assumes that one can distinguish the Green's function in time from the focusing functions. In other words, Marchenko methods work best for limited offset data in layered media where refracted waves and near-surface inhomogeneity zones do not exist. The up/down separation fails if the first arrival waves are not the direct wave (which can happen for example with large-offset data), and leads to unsuccessful imaging attempts (Wapenaar et al., 2014, 2019).

We eliminate the up/down component retrieval for the wavefield to focus on a point in 2D, and retrieve the response to a virtual source at the focal point inside the medium. Our method generalizes the algorithm of Rose (2001, 2002) to two dimensions, and our retrieved Green's function contains all scattering effects of the medium. We present our numerical examples for a closed boundary with a constant background velocity medium; however, if the velocity is allowed to vary, the required causality condition that the perturbed waves arrive after the direct wave may be violated. We model the direct wave in the homogeneous medium for a point source inside the medium, which defines the focal point; we then emit the time-reversal of the modeled direct wave back into the medium from receiver locations; the recorded coda wave information is then used for the next iteration along with the modeled direct wave. We apply an iterative recipe, which uses the direct wave information modeled in the homogeneous medium and the coda information that is time-reversed and propagated from the receivers. We retrieve the virtual Green's function at the focal point including the direct wave and multiply-scattered wave information. We present this approach with numerical examples and compare the results to those obtained from directly modeled responses. Our methodology can be regarded as the first step toward relaxing the need for up/down decomposition in the current Marchenko methods.

## VISUAL TOUR

Figure 1 shows the source and receiver geometry of a 2D acoustic medium. The red dot in Figure 1 denotes the virtual source location and blue dots represent the receiver locations. The virtual source location is given by $x_s = 3.5$ km and $z_s = 1$ km in depth. The medium has a constant background velocity and density, $c_0 = 2$ km/s and $\rho_0 = 2$ g/$cm^3$, respectively. Figure 1 also shows four different elliptical-shaped scatterers located in the subsurface with densities $\rho_1 = 4.5$ g/$cm^3$, $\rho_2 = 5$ g/$cm^3$, $\rho_3 = 7.5$ g/$cm^3$, $\rho_4 = 6$ g/$cm^3$, respectively. We use finite-difference modeling with absorbing boundaries where surface-related multiples are excluded in the modeling. The source wavelet is a Ricker with a central frequency of 20 Hz.

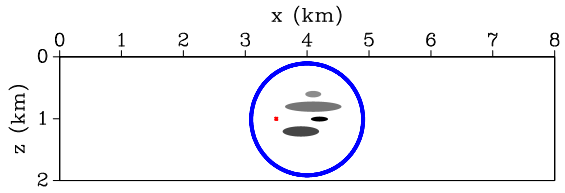


Figure 1: Source and receiver configuration of the 2D model. The red dot shows the virtual source location and the blue dots show the receiver locations in the subsurface. The elliptical scatterers are located inside the receiver array with variable densities.

We define the Green's function, $G(\mathbf{x}, \mathbf{x}_s, t)$, as the solution to the wave equation $LG$=-$\rho\delta(\mathbf{x}-\mathbf{x}_s)\partial\delta(t)/\partial t$, with the differential operator $L = \rho\nabla.(\rho^{-1}\nabla) - c^{-2}\partial^2/\partial t^2$. Here, $\mathbf{x}_s$ is the source location in depth, and the Green's function is the response to a source at $\mathbf{x}_s$ recorded at the receiver location $\mathbf{x}$.

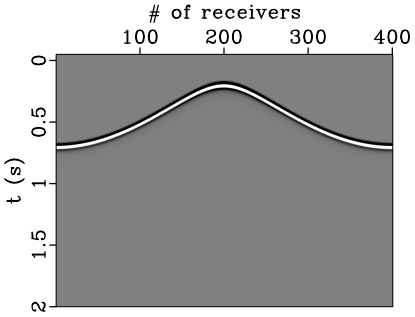


Figure 2: Directly modeled direct wave at the predefined focal point in the homogeneous medium. The receivers are located counter-clockwise direction along the blue circle in Figure 1 with the first receiver coordinates $x = 4.9$ km and $z = 1$ km.

We describe an iterative solution to create a wavefield that focuses to a pre-defined subsurface location at $t = 0$ when injected into the medium. Our solution requires the direct wave information modeled in the homogeneous background medium at the virtual source position which is given by the red dot in Figure 1. The direct wave is the Green's function in the homogeneous medium represented by $U_d(\mathbf{r}, t)$ in Figure 2. Here, $\mathbf{r} = (x, z)$ denotes the coordinates of the receivers that are located in the subsurface and $t$ denotes time.

When the time-reversal of the direct wave is injected into the heterogeneous medium, it creates a focus at the focal point; however, as shown in Figure 3a, in addition to the focal spot, other waves are present at $t = 0$. As shown in Figure 3b, our algorithm creates a wavefield that focuses to the pre-defined subsurface location and eliminates other arrivals at $t = 0$. The iterative scheme starts with the direct Green's function, $U_d(\mathbf{r}, t)$. Time-reversal of the direct Green's function, $U_d(\mathbf{r}, -t)$,

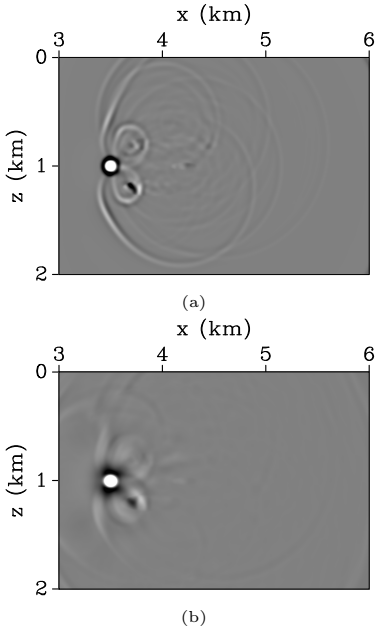


Figure 3: (a) Snapshot at $t = 0$ of the time-reversed modeled direct wave injection. (b) Snapshot at $t = 0$ of the time-reversed retrieved Green's function injection.

is propagated through the heterogeneous medium and the reflected wavefield for the $k$th iteration, $U_k(\mathbf{r}, t)$, is recorded at the receiver positions. Figure 4a shows the recorded wavefield after injecting the time-reversed direct Green's function. We then define a window function, $w(\mathbf{r}, t)$, to keep only the coda information from the recorded data. From the first arriving waves in Figure 2, we specify a time $t^i_{dir}$ such that for every receiver, $\mathbf{r}_i$, the time window only passes waves for $-t^i_{dir} < t < t^i_{dir}$. The $k$th iteration of the coda is given by

$$K_k(\mathbf{r}, t) = w(\mathbf{r}, t)U_k(\mathbf{r}, t). \tag{1}$$

We then define the wavefield for the next iteration as the combination of the time-reversed direct Green's function and the time-reversed coda information. To begin the first iteration, the direct Green's function is time-reversed and injected into the medium. For higher iterations, the iterative solution is given by

$$U^{in}_{k+1}(\mathbf{r}, t) = U_d(\mathbf{r}, -t) + K_k(\mathbf{r}, -t), \tag{2}$$

$$U^{out}_{k+1}(\mathbf{r}, t) = \oint R(\mathbf{r}, \mathbf{r'}, t)U^{in}_{k+1}(\mathbf{r'}, t)dr', \tag{3}$$

where $R(\mathbf{r}, \mathbf{r'}, t)$ is the outgoing wave at location $\mathbf{r}$ caused by a unit ingoing wave at $\mathbf{r'}$, i.e., it is the scattering response of the medium. We then define the coda as

$$K_{k+1}(\mathbf{r}, t) = w(\mathbf{r}, t)U^{out}_{k+1}(\mathbf{r}, t). \tag{4}$$

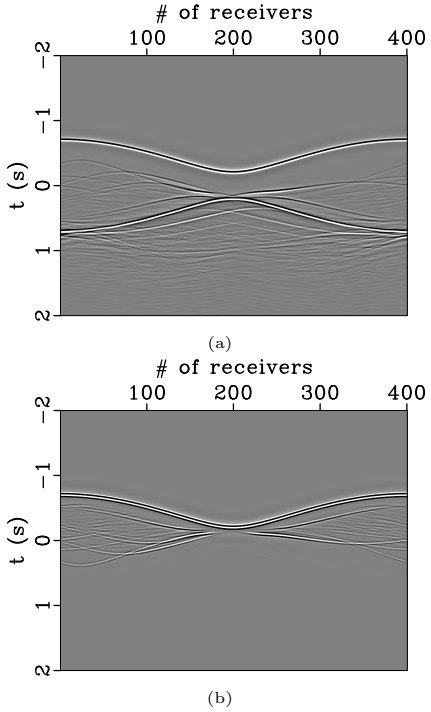


Figure 4: (a) Recorded data after injecting the time-reversed direct wave from the receiver locations. (b) Recorded data after applying time window $w(\mathbf{r}, t)$, time-reversal, and adding the time-reversed direct wave.

Figure 4b shows $U^{in}_{k+1}(\mathbf{r}, t)$ for the first iteration. It is the combination of the time-reversal of the direct Green's function and the coda information of the first iteration. It is the output of the first iteration and also will be the input for the second iteration.

Figure 5 shows the third iteration result and the coda is nearly symmetric for the time interval $-t^i_{dir} < t < t^i_{dir}$. The difference $U_k(\mathbf{r}, t) - U_k(\mathbf{r}, -t)$ will eliminate the waves in the nearly symmetric region in Figure 5. We let $K_k(\mathbf{r}_i, -t)$ be the time-reversed version of $K_k(\mathbf{r}_i, t)$ so that $K_k(\mathbf{r}_i, -t) = K_k(\mathbf{r}_i, t)$ for the time interval $-t^i_{dir} < t < t^i_{dir}$. We obtain the difference solution as

$$U^{(dif)}_k(\mathbf{r}, t) = U_k(\mathbf{r}, t) - U_k(\mathbf{r}, -t). \tag{5}$$

Equation 5 enables us to create the response to a virtual source located in the subsurface at the focal point. Figures 6a and 6b show the wavefields for the first iteration and third iteration, respectively. The iterative solution provides the symmetry region in time (shown in Figure 5) for $-t^i_{dir} < t < t^i_{dir}$, and by taking the difference we obtain a wavefield with canceled coda information that retrieves the Green's function with the focal point as virtual source location shown in Figure 6b. Figure 6c shows the directly modeled Green's function, as a reference.

The Green's function minus its time-reversal is defined

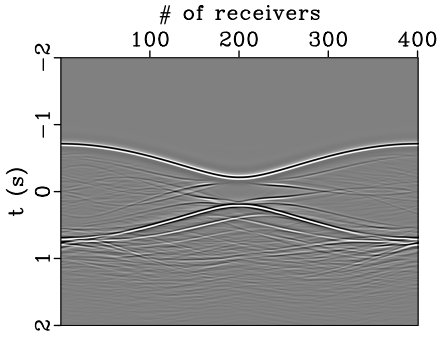


Figure 5: Recorded data after the third iteration with the symmetry region for $-t^i_{dir} < t < t^i_{dir}$.

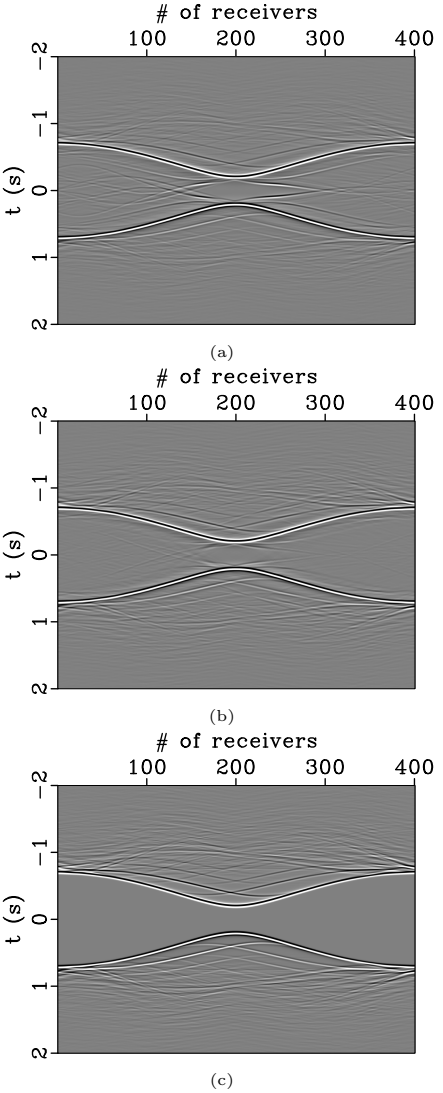


Figure 6: Wavefield $U^{(dif)}_k(\mathbf{r}, t)$ at the receiver array for the first and third iteration shown in (a) and (b), respectively. Wavefields are calculated by $U_k(\mathbf{r}, t) - U_k(\mathbf{r}, -t)$. (c) Directly modeled Green's function minus its time-reversal.

as the homogeneous Green's function by Oristaglio (1989). The match both between the directly modeled homogeneous Green's function and the retrieved Green's function is excellent except for the numerical inaccuracies that reside in the area between the causal and anti-causal part of the retrieved homogeneous Green's function.

Figures 7a and 7b show the traces from the estimated and true Green's functions for the receiver number 200 with coordinates $x = 3.1$ km and $z = 1$ km. Figure 7a shows the traces for positives times only whereas Figure 7b shows the zoomed-in version of Figure 7a. The red trace denotes the directly modeled Green's function and the blue trace denotes the retrieved Green's function. The latest arrival time for the single scattered waves for our geometry is calculated approximately as 1.8 s. Given the geometry, all waves arriving after 1.8 s must be multiply scattered waves only, and for earlier times the Green's function consists of a combination of single scattered waves and multiples. As a result of our iterative solution, we retrieve the direct wave and multiply-scattered wave information, and for both time windows in Figure 7, directly modeled and retrieved Green's functions match very accurately both in time and amplitude.

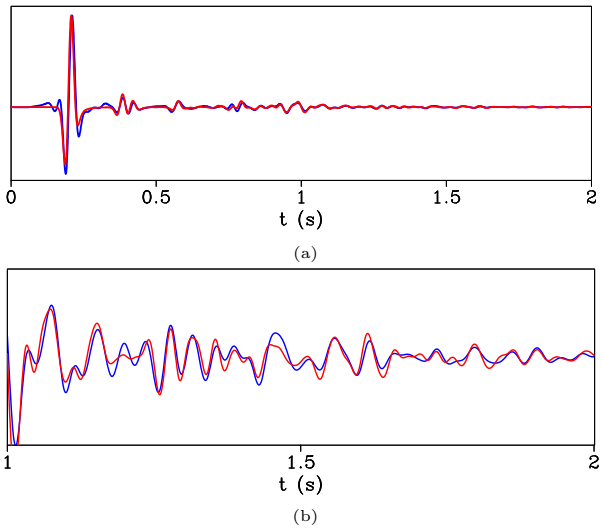


Figure 7: (a) Numerically computed Green's function (red) and the Green's function obtained from our algorithm (blue) for positive times from 0 s to 2 s. (b) Limited time interval of the traces ranging from 1 s to 2 s. Both traces match almost perfectly except for the small amplitude mismatches.

We also inject the time-reversal of the causal part of the difference solution obtained after the third iteration back into the medium from the receiver locations. This retrieved Green's function improves the focusing in the subsurface. Figure 3a shows a snapshot at $t = 0$ of the time-reversed direct wave injection. Following our algorithm, Figure 3b shows a snapshot at $t = 0$ of time-reversed retrieved Green's function injection. In Figure 3b, the target is only a nonzero wavefield at the focal point thus we have a cleaner snapshot than Figure 3a because of the canceled events at $t = 0$ around the focusing location.

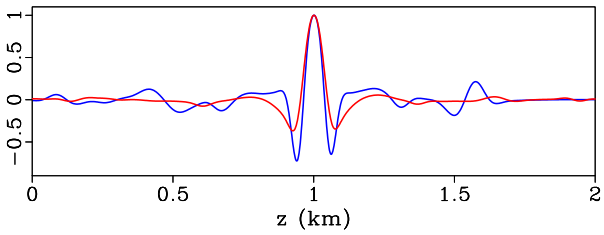


Figure 8: The blue trace shows a vertical cross-section of the snapshot at $x = 3.5$ km in Figure 3a and the red line shows a vertical cross-section of the snapshot at $x = 3.5$ km in Figure 3b. The red trace shows fewer variations because the iterative scheme cancels other disturbing arrivals and solidifies the focus in the subsurface.

The reconstructed Green's function is able to cancel other arrivals while creating a cleaner focus than the direct wave injection in the subsurface. Figure 8 shows normalized vertical cross-sections taken from Figures 3a and 3b for $x = 3.5$ km. The blue trace denotes the cross-section of Figure 3a and the red trace denotes the cross-section of Figure 3b. The blue trace in Figure 8 shows variations along the cross-section whereas the red trace shows a more stable cross-section due to the canceled events and improved focus at the focal point.

## CONCLUSIONS

We present a visual tour for explaining the focusing process without up/down decomposition. We show that we can create better focusing in the subsurface by $U_k(\mathbf{r}, t) - U_k(\mathbf{r}, -t)$ than one can achieve with the direct waves only (see Figure 3). We successfully retrieve the Green's function for a pre-defined subsurface location and the comparison to the directly modeled Green's function is found to be excellent. Our retrieved Green's function retrieves both the primary and multiple events of the heterogeneous subsurface model. The iterative method we present converges at three iterations; however, more iterations might be needed for more complex subsurface models. The iterative scheme we propose forms the basis for imaging without up/down decomposition, and makes the Marchenko methods more appropriate for imaging dipping structures.

## ACKNOWLEDGMENTS

This work is supported by the Consortium Project on Seismic Inverse Methods for Complex Structures at the Colorado School of Mines. The reproducible numeric examples in this paper were generated using the Madagascar software package (http://www.ahay.org).

## REFERENCES

Broggini, F., and R. Snieder, 2012, Connection of scattering principles: A visual and mathematical tour: European Journal of Physics, **33**, no. 3, 593–613.

Broggini, F., R. Snieder, and K. Wapenaar, 2012, Focusing the wavefield inside an unknown 1D medium: Beyond seismic interferometry: Geophysics, **77**, no. 5, A25–A28.

———, 2014, Data-driven wavefield focusing and imaging with multidimensional deconvolution: Numerical examples for reflection data with internal multiples: Geophysics, **79**, no. 3, WA107–WA115.

Oristaglio, M. L., 1989, An inverse scattering formula that uses all the data: Inverse Problems, **5**, no. 6, 1097–1105.

Rose, J. H., 2001, "Single-sided" focusing of the time-dependent Schrödinger equation: Physical Review A, **65**, no. 1, 012707.

———, 2002, Time reversal, focusing and exact inverse scattering. in: Fink m., kuperman w.a., montagner jp., tourin a. (eds) imaging of complex media with acoustic and seismic waves. topics in applied physics, vol 84: Springer, Berlin, Heidelberg.

Wapenaar, K., J. Brackenhoff, and J. Thorbecke, 2019, Green's theorem in seismic imaging across the scales: Solid Earth, **10**, no. 2, 517–536.

Wapenaar, K., J. Fokkema, and R. Snieder, 2005, Retrieving the Green's function in an open system by cross correlation: A comparison of approaches (L): The Journal of the Acoustical Society of America, **118**, no. 5, 2783–2786.

Wapenaar, K., J. Thorbecke, J. van der Neut, F. Broggini, E. Slob, and R. Snieder, 2014, Marchenko imaging: Geophysics, **79**, no. 3, WA39–WA57.

Weaver, R., and O. Lobkis, 2001, Ultrasonics without a source: Thermal fluctuation correlations at MHz frequencies: Physical Review Letters, **87**, no. 13, 134301.